Available online at www.sciencedirect.com
ScienceDirect
Ceramics International 36 (2010) 1455–1461
CERAMICS INTERNATIONAL
www.elsevier.com/locate/ceramint

Development and characterisation of triaxial electrical porcelains from Ugandan ceramic minerals

Peter W. Olupot [a,b], Stefan Jonsson [a,*], Joseph K. Byaruhanga [b]

[a] Department of Material Science and Engineering, Royal Institute of Technology (KTH), Brinellvägen 23, SE-100 44 Stockholm, Sweden
[b] Department of Mechanical Engineering, Faculty of Technology, Makerere University, P.O. Box 7062, Kampala, Uganda

Received 1 December 2009; received in revised form 9 December 2009; accepted 25 January 2010
Available online 1 March 2010

Abstract

Ten formulations of triaxial porcelain composed from 30–60% clay, 20–45% feldspar and 20–25% sand, were prepared from raw materials sourced from Ugandan deposits. Specimens were made using the plastic extrusion method and characterized in terms of constituent oxide composition, flexural strength, fracture toughness, dielectric strength, microstructure and phase properties using ICP-AES analyses, 4-point load strength test, Vicker's indentation, FEG-SEM and powder-XRD analyses, respectively. XRD studies revealed that the crystalline phases are mullite and quartz and their intensity is almost identical for all samples fired at 1250 °C but there is a decrease in quartz content as temperature is increased. Samples with 20% sand content resulted in higher density, modulus of rupture and fracture toughness compared to those containing 25% sand. The major factor influencing bending strength was found to be porosity in samples as opposed to crystallinity. A sample with 67.3% SiO_2, 20.2% Al_2O_3, 3.4% K_2O and 6.3% others exhibited best properties.

Keywords: C. Dielectric properties; C. Mechanical properties; D. Porcelain; Ceramic raw materials

1. Introduction

Triaxial porcelain forms a large base of the commonly used porcelain insulators for both low and high tension insulation. It is considered to be one of the most complex ceramic materials and most widely studied ceramic system [1], yet there still remains significant challenges in understanding it in relation to raw materials, processing science, phase and microstructure evolution [2]. It is made from a mixture of the minerals clay, quartz, and feldspar. The clay [$Al_2Si_2O_5(OH)_4$], give plasticity to the ceramic mixture; flint or quartz (SiO_2), maintains the shape of the formed article during firing; and feldspar [$K_xNa_{1-x}(AlSi_3)O_8$], serves as flux. These three constituents place this porcelain in the phase system [$(KNa)_2O$–Al_2O_3–SiO_2)] in terms of oxide constituents [3]. The fired porcelain product contains mullite ($Al_6Si_2O_{13}$) and undissolved quartz (SiO_2) crystals embedded in a continuous glassy phase, originating from feldspar and other low melting impurities in the raw materials. Each phase has its specific influence on the mechanical and dielectric properties of the body depending on its concentration and microstructural attributes [4]. Microstructural attributes and concentration of the phases are largely influenced by temperature and compositional differences [5,6].

The effects of the individual phases on the mechanical properties have been elucidated under the mullite hypothesis, the matrix reinforcement and the dispersion strengthening hypotheses [2,7]. None of these hypotheses seems satisfactory on its own in explaining the strength of triaxial porcelains, thus providing a range of material 'recipes' for electric porcelain products, typically 30–60% clay, 15–35% feldspar and 20–40% quartz [3,8,9]. This is partly also due to the wide variation in the chemical composition of the raw materials used.

An earlier study on triaxial porcelain from Ugandan minerals by the present authors [10] on samples fired at different temperatures revealed the difficulty in extruding specimens with 30% sand and established best properties after firing to a temperature of 1250 °C. In the present study, 10 formulations of porcelain were prepared and specimens produced from them using the plastic extrusion method. The specimens were fired at a temperature of 1250 °C and characterized in terms of flexural strength, dielectric strength,

* Corresponding author. Tel.: +46 8 790 89 49; fax: +46 8 20 31 07.
E-mail addresses: polupot@tech.mak.ac.ug (P.W. Olupot), jonsson@kth.se (S. Jonsson), jbyaruhanga@tech.mak.ac.ug (J.K. Byaruhanga).

0272-8842/$36.00
doi:10.1016/j.ceramint.2010.02.006

Table 1
Chemical composition of raw materials (wt%).

Compound	Kaolin	Ball-clay	Feldspar	Sand
SiO_2	56.60	65.70	64.60	91.70
Al_2O_3	31.50	17.10	19.60	2.94
CaO	0.80	0.28	0.29	2.29
Fe_2O_3	0.71	2.69	0.23	1.71
K_2O	1.78	0.83	10.10	0.54
MgO	0.30	0.32	0.04	0.73
MnO	0.01	0.02	0.01	0.03
Na_2O	0.26	0.28	0.96	0.53
P_2O_5	0.07	0.06	0.06	0.12
TiO_2	0.09	1.89	0.04	0.31
LOI	10.40	8.00	2.80	1.70
Total	102.52	97.17	98.73	102.60

LOI represents loss on ignition.

fracture toughness, along with microstructural and phase properties. The aim was to establish a material mix formulation, based on Ugandan minerals, hitherto unknown for successful application in the triaxial porcelains, with a combination of good mechanical and electrical properties and to describe it in terms of the resultant microstructure.

2. Materials and experimental procedures

2.1. Raw materials

The raw materials used were ball-clay from Mukono, kaolin and feldspar from Mutaka and sand from Lido beach on the shores of Lake Victoria in Entebbe, Uganda. These deposits and their locations are described elsewhere [11,12]. Representative samples were collected from the deposits and processed for use in the study. The mineralogical compositions of the processed materials are given in Table 1. Admittedly, the total sum of oxides for each material is not exactly 100% due to experimental uncertainties.

2.2. Sample preparation

The materials were each separately wet-milled, run over a magnetic iron separating tray to remove iron contamination and sieved through aperture sizes of 45 μm for kaolin and ball-clay, 53 μm for feldspar and 25 μm for sand. The aperture sizes were selected on the basis of cited literature on improvement of porcelain strength [13–15]. The materials were subsequently dried with the exception of ball-clay which was mixed as slip in the composition. The dry content of the ball-clay in the slurry was calculated using Brogniart's formula [16].

Ten compositions were formulated with clay content of 35–60%, feldspar 20–45% and sand 20–25%. Previous investigations [10] on samples of 30% sand did not yield bodies with good plasticity for extrusion, hence bodies with sand content of 30% were left out from this study. The ball-clay content was maintained at ≈33% of the total clay content, so as to limit excessive drying shrinkage. Respective batches (Table 2) were mixed in required proportions by weight and wet-milled in a ball mill with a quartz grinding medium for 3 h.

Table 2
Sample composition (wt%).

Sample	A	B	C	D	E	F	G	H	I	J
Kaolin	23	27	30	33	37	40	27	30	33	37
Ball-clay	12	13	15	17	18	20	13	15	17	18
Feldspar	45	40	35	30	25	20	35	30	25	20
Sand	20	20	20	20	20	20	25	25	25	25
Total	100	100	100	100	100	100	100	100	100	100

In preparation for extrusion, the milled materials were left to dry at room temperature to form a paste of sufficient plasticity for extrusion through a de-airing pugmill. The extruder was washed clean after every batch. Extruded cylindrical specimens of 15 mm diameter were, upon drying cut to 80 mm length. They were then dried in an oven at a temperature of 120 °C for 24 h. Dried samples from each batch were fired to a temperature of 1250 °C at a heating rate of 6 °C/min and held at the maximum temperature for 1 h, cooled at 6 °C/min to 500 °C and let to cool to room temperature in the furnace. Selected samples were fired to temperatures of 1300 °C and 1350 °C to study the effect of temperature on the microstructure.

2.3. Measurements and observations

Firing shrinkage of the samples was determined by measuring the diameter and length of the samples before and after firing and expressing the difference as a percentage of the values before firing. The results reported are an average of the diametral and the lengthwise shrinkage.

Bulk density was determined from measurements of volume and mass of fired samples. Bending strength was measured using a strength testing machine (Model M500, Testometric Universal Testing Machine, UK) in a 4-point load bending fixture for the as-fired specimens. The crosshead speed was 1 mm/min and the spans between the upper and lower supports were 20 mm and 40 mm, respectively. A minimum of 15 specimens were tested for each sample. The reported figures of modulus of rupture (MOR) were evaluated using Weibull statistics according to the assumptions described in our earlier work [10].

Fracture toughness (K_{IC}) was evaluated for polished specimen surfaces by the indentation technique in a Vickers micro-hardness tester. A minimum of five indentations were made on each specimen. The instrument was adjusted to deliver a load of 1 kgf for 15 s. The diameter of radial cracks was measured immediately after indentation. Crack length measurements were only made on indents that were well defined without chipping and for which the cracks did not terminate at pores. Two measurements were made for each indentation and the average of 10 readings used to evaluate the value of K_{IC} for each sample. K_{IC} was calculated from the formula given by Evans and Wilshaw as cited by Baharav et al. [17] in the following equation:

$$K_{IC} = \frac{1}{\pi^{3/2}\tan\psi}\left(\frac{P}{D^{3/2}}\right)$$

Table 3
Calculated chemical composition of the samples (wt%).

Sample	A	B	C	D	E	F	G	H	I	J
SiO_2	68.31	68.00	67.79	67.57	67.26	67.04	69.36	69.14	68.92	68.61
Al_2O_3	18.71	19.16	19.46	19.77	20.22	20.53	18.32	18.63	18.94	19.39
CaO	0.81	0.83	0.84	0.86	0.88	0.89	0.93	0.94	0.96	0.98
Fe_2O_3	0.93	0.98	1.04	1.10	1.15	1.21	1.05	1.11	1.18	1.22
K_2O	5.16	4.74	4.30	3.87	3.44	3.01	4.26	3.82	3.39	2.96
MgO	0.27	0.28	0.30	0.31	0.32	0.34	0.32	0.33	0.35	0.36
MnO	0.02	0.02	0.02	0.02	0.02	0.02	0.02	0.02	0.02	0.02
Na_2O	0.63	0.60	0.56	0.53	0.49	0.46	0.58	0.54	0.51	0.47
P_2O_5	0.07	0.07	0.08	0.08	0.08	0.08	0.08	0.08	0.08	0.08
TiO_2	0.33	0.35	0.39	0.43	0.45	0.48	0.36	0.40	0.44	0.46
LOI	4.95	5.31	5.64	5.97	6.33	6.66	5.25	5.59	5.92	6.27
Total	100.19	100.32	100.41	100.49	100.63	100.71	100.52	100.60	100.68	100.82

where K_{IC} is the fracture toughness, ψ is the indenter cone angle (68°), P is the peak contact load and D is the radius of radial crack.

Using pulverised dried material from the extrusion process, samples for dielectric strength tests were prepared by uniaxial pressing at 100 MPa to form discs of 3 ± 0.5 mm thick and 50 mm diameter. All the samples were dried in air and then at 110 °C for 24 h in an electric furnace. Samples from each batch were then fired to a temperature of 1250 °C at a heating rate of 6 °C/min and held at the top temperature for 1 h, cooled at 6 °C/min to 500 °C and let to cool to room temperature in the furnace, with the furnace switched off.

The microstructures of selected samples were observed using a Field Emission Gun Scanning Electron Microscope (FEG-SEM), LEO 1530 with a GEMINI column. Specimen surfaces were polished, etched by dipping in 40% concentrated hydrofluoric acid for 25 s, washed in water and acetone and then dried.

The phase assembly in the fired porcelain samples were determined by X-ray diffraction using X'pertPRO PANalytical X-ray diffractometer, PW 3050/60, with a Ni-filtered Kα Cu-radiation operated at 45 kV and 40 mA. The equipment was operated at a scan speed of 0.108° s^{-1} from 5 to 100°.

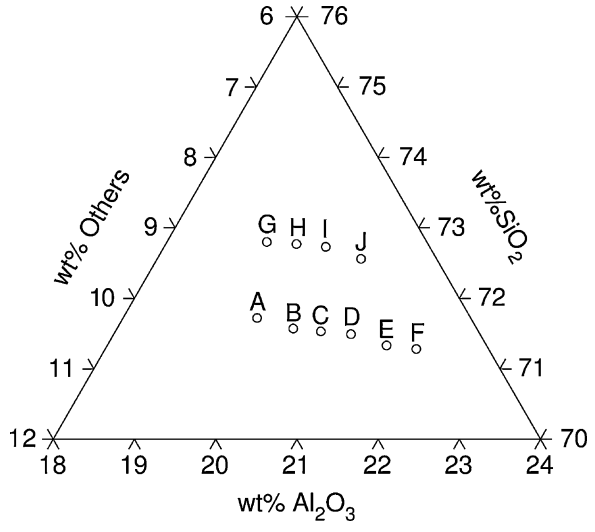

Fig. 1. Samples on triaxial plot of major oxides and the sum of the others.

3. Results

3.1. Chemical analysis

The calculated chemical composition of the samples, found by combining the material chemical composition (Table 1) and the batch weights (Table 2) are as indicated in Table 3. The sum of oxides for each sample is not exactly 100% due to the effect of the chemical analysis results, presented in Table 1.

In terms of the major oxide contents, the formulated porcelain bodies are presented in Fig. 1 in the triaxial plot. The figure indicates that the formulated compositions lay in the range of 71–73% SiO_2, 19–22% Al_2O_3 and 7–9% others, excluding loss on ignition.

3.2. Shrinkage, bulk density, MOR and K_{IC}

The results from shrinkage, bending tests (MOR), bulk density and fracture toughness (K_{IC}) of samples sintered at 1250 °C, are shown in Figs. 2–5. For Figs. 2–6, clay content is the sum of kaolin and ball-clay contents in the individual

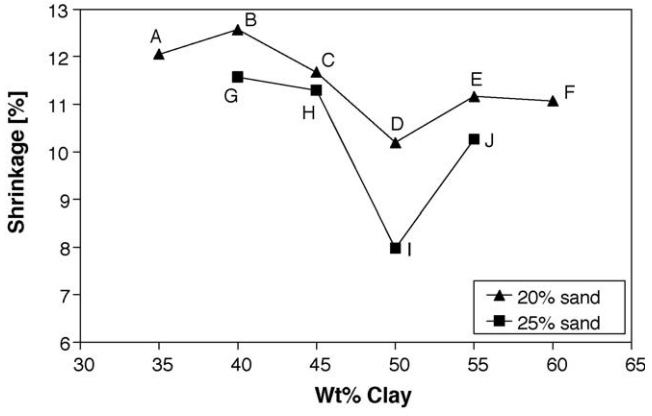

Fig. 2. Shrinkage of samples fired to 1250 °C, with 1 h soaking at peak temperature.

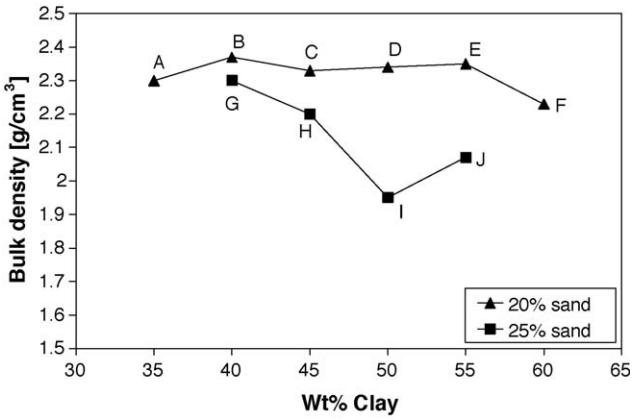

Fig. 3. Bulk density of samples fired to 1250 °C, with 1 h soaking at peak temperature.

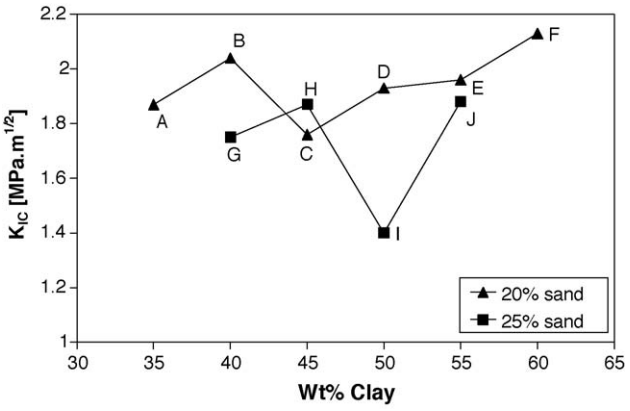

Fig. 5. Fracture toughness of samples fired to 1250 °C, with 1 h soaking at peak temperature.

bodies. The results are grouped in two series, one for 20% sand and the other for 25%. As seen, the results for 20% sand generally show the highest test values for all properties. Probably, the reason for this behavior should be looked for in the sintered microstructure, and will be discussed later. Actually, it is not surprising that the 20%-series, having the highest shrinkage, also obtains the highest bulk density and MOR, since they are intimately related to each other. A good consolidation leads to a high bulk density, less defects and an increased bending strength. The K_{IC} values, on the other hand, show the fracture toughness of defect-free material and must be related to the intrinsic properties of the glass phase and its embedded crystallites.

As seen from Figs. 2 and 3, the shrinkage and bulk density show a weak variation with the amount of clay. The same trends are found in both figures because of the intimate coupling between the two properties. By some reason, specimen I seems to have poorer consolidation than the rest of the specimens. By comparing with Figs. 4 and 5, it is interesting to note that a deviation is also found for specimen I for K_{IC} but not for MOR. This is unexpected since poor consolidation generally is accompanied by poor MOR. A similar unexpected deviation is found for specimens C and H. Both specimens show good consolidation and K_{IC} but poor MOR. Then, evidently, MOR is determined by both defect characteristics and bulk matrix properties.

3.3. Dielectric strength

The variation of dielectric strength with composition of the samples is shown in Fig. 6. Above 45% clay content, the dielectric strength increase with increase in clay content irrespective of the sand content. The strength values obtained for the samples are all within or above the range of 6.1–13 kV/mm, which is the specified range for porcelain insulators [3]. Generally, the relative changes in dielectric strength values for the samples are very small.

3.4. Microstructure

Specimens B, E and J, showing high MOR-values were selected for microstructure analyses. The amount of pores and the appearance of the mullite crystallites are shown in Figs. 7 and 8 after sintering at 1250 °C and 1300 °C. Clearly, specimens B and E have lower amount of pores than specimen J, which is consistent with their higher MOR-values. The K_{IC}-

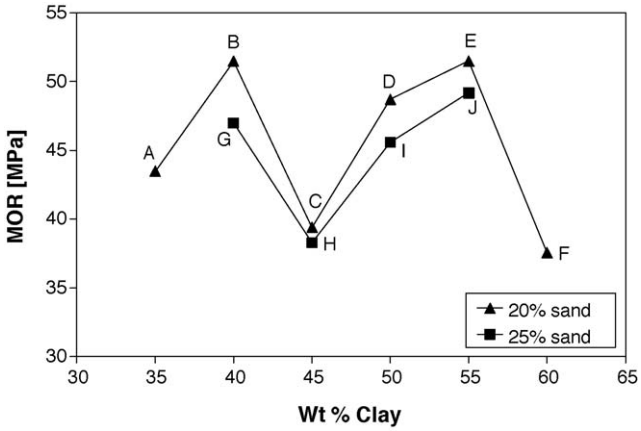

Fig. 4. Modulus of rupture of samples fired to 1250 °C, with 1 h soaking at peak temperature.

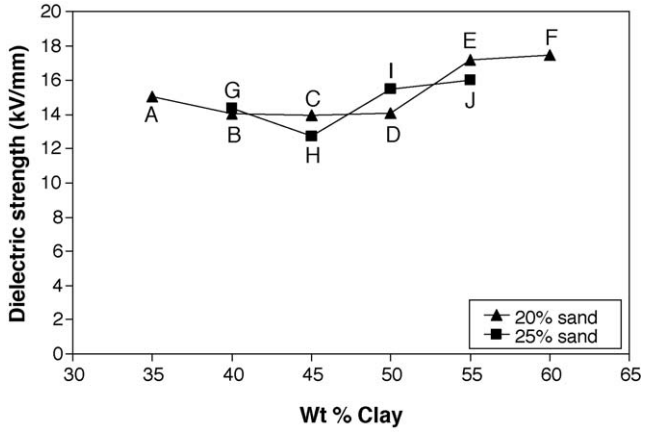

Fig. 6. Dielectric strengths of samples fired to 1250 °C, with 1 h soaking at peak temperature.

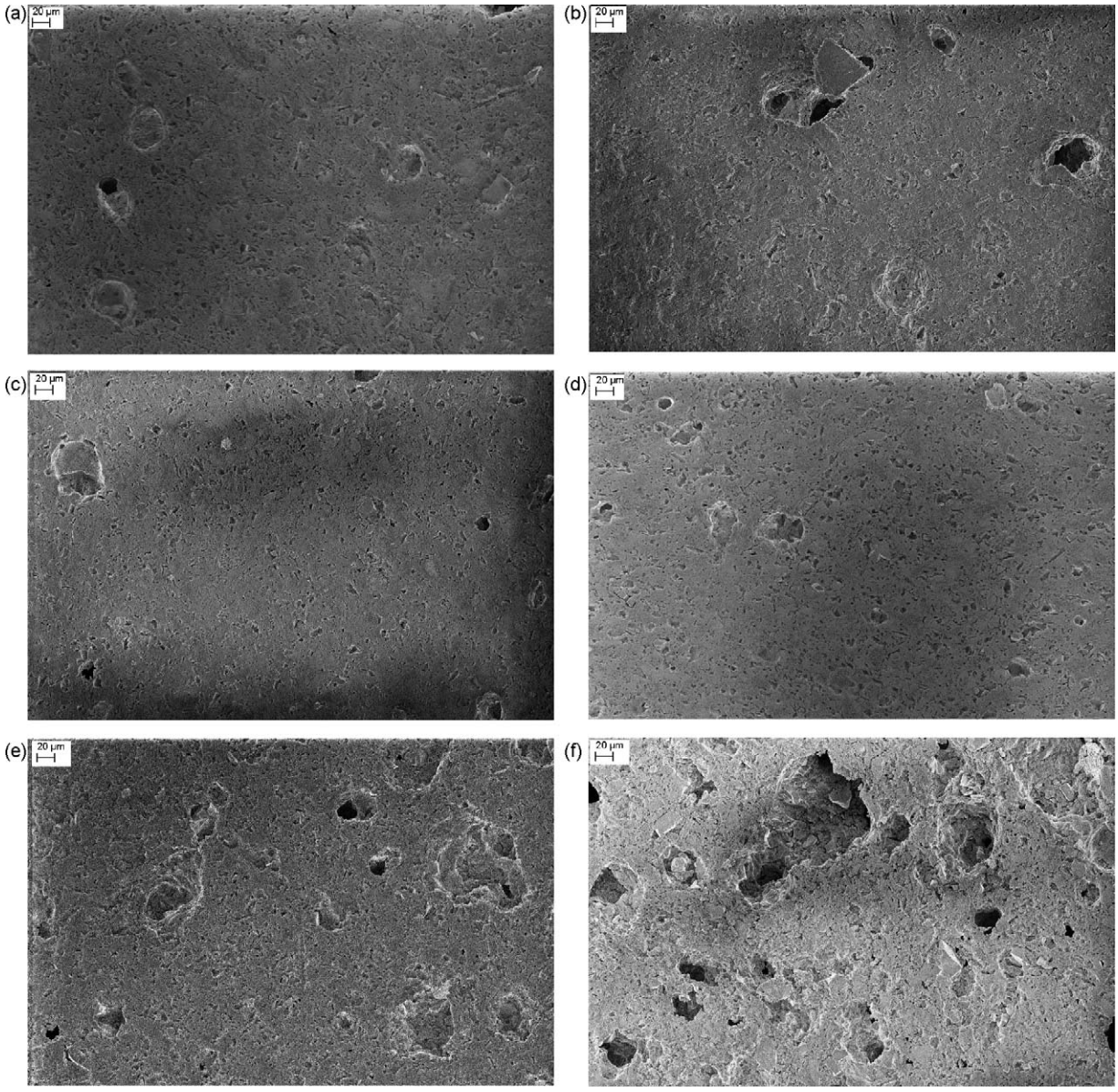

Fig. 7. SEM micrographs of (a) B sintered at 1250 °C, (b) B sintered at 1300 °C, (c) E sintered at 1250 °C, (d) E sintered at 1300 °C, (e) J sintered at 1250 °C, and (f) J sintered at 1300 °C.

values follow the same trend even if they are measured on defect-free material. However, the difference between the specimens is not big, which is consistent with the microstructures shown in Fig. 8 showing a similar appearance of the mullite crystals in all specimens.

All specimens consist of quartz and mullite as the major crystalline phases (Figs. 9 and 10), accompanied by a vitreous phase and pores (Figs. 7 and 8). The intensity of the quartz peaks decrease with temperature (Fig. 9). This indicates the dissolution of quartz at high firing temperature resulting in an increase in the vitreous phase reflected by the increase in the bump between angles of 20 and 30°. This was reported in earlier studies by Olupot et al. [10], to lead to decrease in strength of porcelains in accordance with the matrix reinforcement hypothesis [2]. Fig. 10 reveals almost identical intensities for samples fired at 1250 °C, suggesting that the difference in amount of crystalline phase in the microstructure is not the main cause of MOR variation.

4. Discussions

From Figs. 2–5, samples B and E show higher MOR, good value of K_{IC} and higher density. The results obtained from sample B agree with the findings of Correia et al. [18] who, based on statistical modeling, suggested that equal contents of feldspar and clay lead to a body with high bulk density and MOR. The oxide compositions of samples B and E are quite close, and similar to the best formulation in an earlier work [10]. This proves that similar characteristics can be obtained with bodies on the basis of oxide composition rather

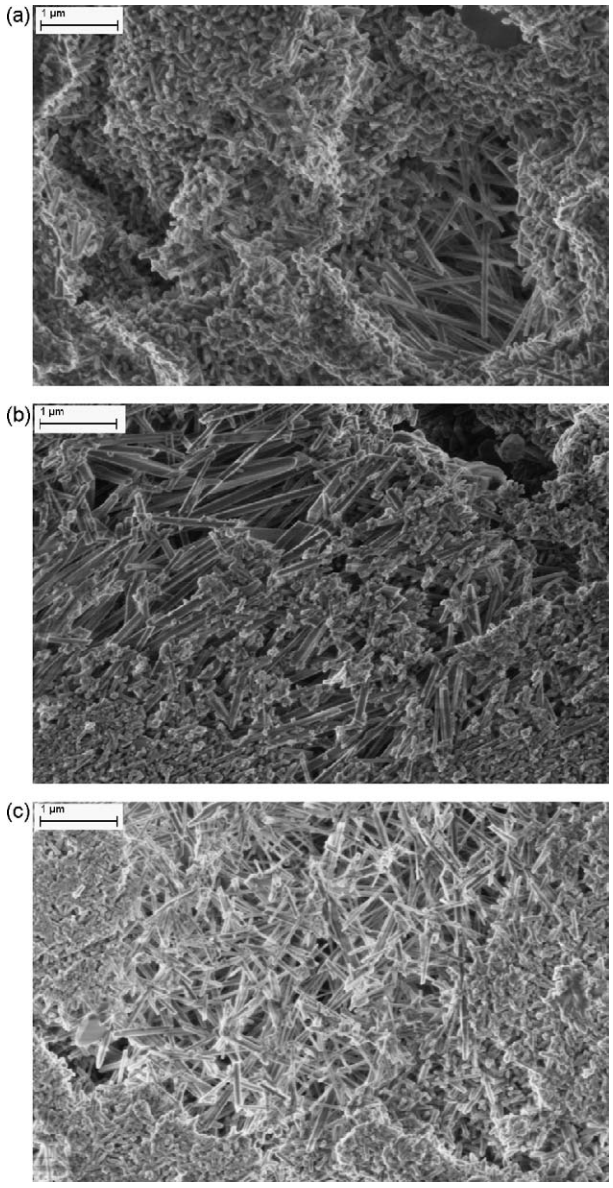

Fig. 8. SEM Microstructure of (a) B sintered at 1250 °C, (b) E sintered at 1250 °C, and (c) J sintered at 1250 °C.

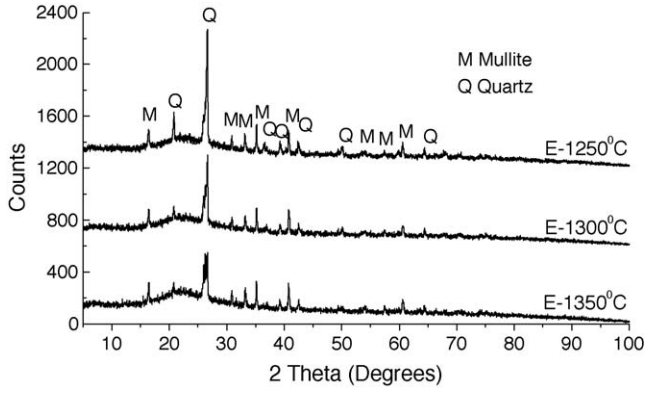

Fig. 9. Powder diffractograms of sample E fired to 1250 °C, 1300 °C, and 1350 °C with 1 h soaking at each peak temperature. For clarity, the curves are shifted vertically by equal proportions from each other.

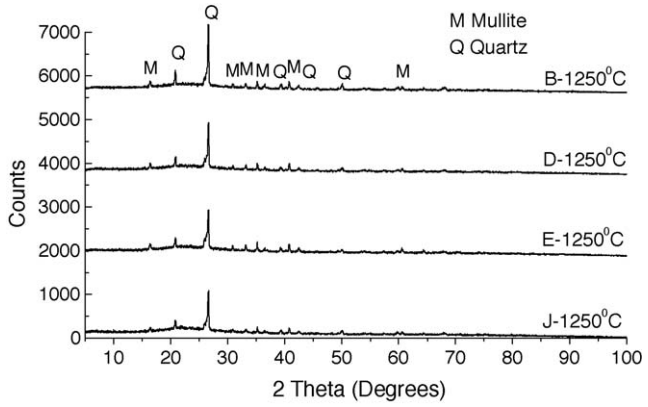

Fig. 10. Powder diffractograms of samples B, D, E and J fired to 1250 °C, with 1 h soaking at peak temperature. For clarity, the curves are shifted vertically by equal proportions from each other.

than the batch weights of raw minerals. A composition of 67.26% SiO_2, 20.22% Al_2O_3, and 3.44% K_2O here exhibits good properties. Use of oxide composition for generating batch weights is thus a more reliable form of specification that can be used to obtain consistent quality porcelains in cases where the compositions of the starting minerals vary.

The results also show that shrinkage increases with reduced sand content. High shrinkage results into a more dense body with a high strength. High porosity at increased firing temperature is due to release of oxygen from the decomposition of Fe_2O_3 and gas expansion within pores [19]. Pore volume expansion occurs as a result of high pressure at high temperature of the released and entrapped gases within the pores. This explains the micrograph of sample J at 1300 °C compared to that at 1250 °C. Sample J possesses the highest Fe_2O_3 of all the samples in Fig. 7.

MOR and K_{IC} values obtained are typical for triaxial porcelains under the 4-point bending load test. It is to be noted that values for this fixture are ∼30% lower than those obtained in the 3-point load fixture [14,20]. For a ceramic material, the breaking stress σ, is related to the applied stress intensity factor at fracture K_{IC}, by $\sigma = K_{IC}/YC^{1/2}$ where C is the flaw size and Y is the geometry factor [21]. The increase in σ may thus be explained by an increase in K_{IC} and/or a decrease in C. Wiederhorn and Fuller [21] further report that the mechanisms involved in increasing K_{IC} work primarily by lowering the crack tip stress concentration. Since the crack tip will not propagate until the crack tip stresses reach the ultimate strength of the material, the force required to drive the crack will be higher for polycrystalline materials than for glasses of the same size crack. Besides crystallinity, deflection of the crack as it propagates, interlocking of grains across the propagating crack, a phase transformation or micro-cracking of grains around the crack tip can give rise to stresses that oppose crack advance thus requiring higher stress for failure. These mechanisms of crack tip shielding in which the load for fracture is transferred from the crack tip to other parts of the microstructure influence fracture toughness

in porcelains. Although there was K_{IC} variation within the samples, there are no significant differences in the intensity of crystallinity (Fig. 9), hence variation of K_{IC} and σ, cannot fully be attributed to variation in crystallinity. On the other hand, there is a correlation between densities of the samples with K_{IC}. Fig. 7 and strength values for sample J at 1250 °C (49.18 MPa) and 1300 °C (28.41 MPa) confirm that high crystallinity and reduction in porosity play an important role for the increase in MOR.

The fired porcelain samples consist of mullite, quartz and glassy phases. The dielectric strength of the samples can only be explained by the specific role played by each of these phases in addition to crystal size and size distribution, which influence the passage of current through the body. The two phases, quartz and glass are insulators by themselves at room temperature [4]. Mullite phase is reported to be a more conducting phase because of the presence of O^{2-} vacancies in its structure [4]. From Figs. 7–10 for specimens fired at 1250 °C, the mullite crystal morphologies appear similar. Fig. 6 generally shows a similar trend for dielectric strength. The increase in dielectric strength with clay content >45% can probably be attributed to the composition of resultant microstructure formed in the fired porcelain body.

5. Conclusions

Mechanical strength and electrical breakdown strength of porcelains formulated within the range of 30–60% clay, 20–45% feldspar and 20–25% sand have been studied. XRD studies revealed that the crystalline phases formed in sintered specimens are mullite and quartz. The intensity of the crystalline phases is almost identical for all samples fired at 1250 °C but there is a decrease in quartz content with the increase of temperature. The magnitudes of modulus of rupture values for these samples, however, differ widely. This suggests that the difference in amount of crystalline phase in the microstructure is not the main cause of modulus of rupture variation. The major factor influencing the strength was found to be pore distribution in the sample as opposed to the crystallinity. Samples with 20% sand content resulted in higher density, modulus of rupture and fracture toughness compared to those containing 25% sand. This effect was a result of formation of dense microstructures in samples with 20% sand. The dielectric strength improved in samples with clay content above 45%, probably due to the composition of resultant microstructure formed in the fired porcelain body. Sample B, containing similar amount of feldspar and kaolin resulted in good mechanical strength properties, confirming results of earlier studies based on statistical modeling [18]. The MOR results for samples B and E, although different in batch formulation from our earlier study, compared very well. These samples have almost similar oxide compositions. This confirms that a more precise approach to specifying the composition of bodies is by use of oxide constituents rather than batch weights of the raw minerals.

Acknowledgements

The authors appreciate the support from the Sida/SAREC-Makerere University Collaborative Research Programme for fully financing the study. They are also grateful to the following collaborators; Royal Institute of Technology (KTH, Sweden), the School of Graduate Studies, Makerere University, Uganda and Uganda Electricity Transmission Company.

References

[1] K. Dana, S. Das, K.S. Das, Effect of substitution of fly ash for quartz in triaxial Kaolin–Quartz–Feldspar system, J. Eur. Ceram. Soc. 24 (2004) 3169–3175.
[2] W.M. Carty, U. Senapati, Porcelain-raw materials, processing, phase evolution and mechanical behaviour, J. Am. Ceram. Soc. 81 (1) (1998) 3–20.
[3] R.C. Buchanan, in: R.C. Buchanan (Ed.), Properties of Ceramic Insulators, Ceramic Materials for Electronics, 2nd ed., Marcel Dekker Inc., New York, 1991.
[4] S.P. Chaudhuri, P. Sarkar, A.K. Charkraborty, Electrical resistivity of porcelain in relation to constitution, Ceram. Int. 25 (1999) 91–99.
[5] Y. Iqbal, W.E. Lee, Microstructural evolution in triaxial porcelain, J. Am. Ceram. Soc. 83 (12) (2000) 3121–3127.
[6] Y. Iqbal, W.E. Lee, Fired porcelain microstructures revisited, J. Am. Ceram. Soc. 82 (12) (1999) 3584–3590.
[7] L. Mattyasovszky-zsolnay, Mechanical strength of porcelain, J. Am. Ceram. Soc. 40 (9) (1957) 299–306.
[8] A.J. Moulson, J.M. Herbert, Electroceramics, 2nd ed., John Wiley & Sons, England, 2003.
[9] F.H. Norton, Fine Ceramics, Technology and Applications, McGraw-Hill Book Co., New York, 1970, pp. 387–407.
[10] P.W. Olupot, S. Jonsson, J.K. Byaruhanga, Effects of mixing proportions and firing temperature on properties of electric porcelain from Ugandan minerals, Ind. Ceram. 28 (1) (2008) 1–10.
[11] P.W. Olupot, S. Jonsson, J.K. Byaruhanga, Characterization of Feldspar and Quartz raw materials in Uganda for manufacture of electrical porcelains, J. Aust. Ceram. Soc. 42 (1) (2006) 29–35.
[12] J.B. Kirabira, S. Jonsson, J.K. Byaruhanga, Powder characterization of high temperature ceramic raw materials in the Lake Victoria region, Silicate Ind. 70 (9–10) (2005) 127–134.
[13] O.I. Ece, Z. Nakagawa, Bending strength of porcelains, Ceram. Int. 28 (2002) 131–140.
[14] S.R. Bragança, C.P. Bergmann, A view of whitewares mechanical strength and microstructure, Ceram. Int. 29 (2003) 801–806.
[15] G. Stathis, A. Ekonomakou, C.J. Stournaras, C. Ftikos, Effect of firing conditions, filler grain size and quartz content on bending strength and physical properties of sanitary ware porcelain, J. Eur. Ceram. Soc. 24 (2004) 2357–2366.
[16] H. Norsker, J. Danisch, Glazes: For the Self-Reliant Potter, Friedr. Vieweg & Sohn Verlagsgesellschaft mbH, Braunschweig, Germany, 1993, pp. 169.
[17] H. Baharav, B. Laufer, R. Pilo, Effect of glaze thickness on the fracture toughness and hardness of alumina-reinforced porcelain, J. Prosthet. Dent. 81 (1999) 515–519.
[18] S.L. Correia, A.P.N. Oliveira, D. Hotza, A.M. Segadães, Properties of triaxial porcelain bodies: interpretation of statistical modeling, J. Am. Ceram. Soc. 89 (11) (2006) 3356–3365.
[19] C.B. Ustundag, Y.K. Tur, A. Capoglu, Mechanical behaviour of low-clay translucent whiteware, J. Eur. Ceram. Soc. 26 (2006) 169–177.
[20] Breviary Technical Ceramics, Properties, http://www.keramverband.de/brevier_engl/5/3/3/5_3_3_1.htm, Accessed August 3, 2009.
[21] S.M. Wiederhorn, E.R. Fuller JR, Structural behaviour of ceramics, in: I. Milne, R.O. Ritchie, B.L. Karihaloo (Eds.), Comprehensive Structural Integrity, vol. 2, Elsevier Science Ltd., 2002, pp. 1–26.